Cell Reports
Physical Science

Article

Discovery of a new coreactant for highly efficient and reliable electrochemiluminescence

Graphical abstract

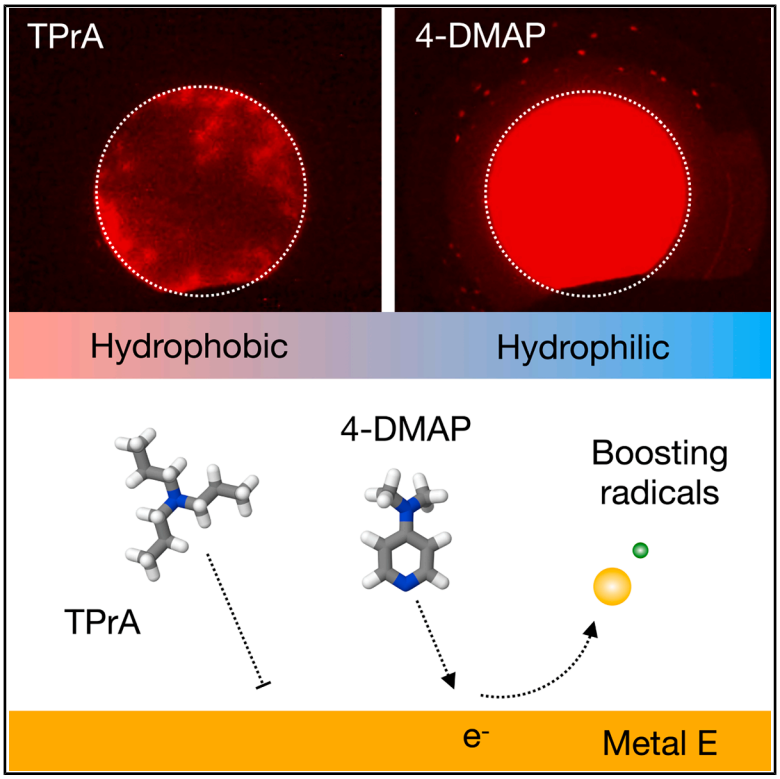

Authors

Young Kwan Cho, Sang-Hyun Jeon, Jung Yeon Park, ..., Jong-Seo Kim, Hakho Lee, Ik-Soo Shin

Correspondence

hlee@mgh.harvard.edu (H.L.), extant@ssu.ac.kr (I.-S.S.)

In brief

The sensitivity of electrochemiluminescence (ECL) assays relies on effective luminophore-coreactant pairs. Cho et al. introduce 4-(dimethylamino)pyridine (4-DMAP), a stable, water-soluble coreactant that enhances $[Ru(bpy)_3]^{2+}$ ECL by over 180-fold compared to tri-*n*-propylamine (TPrA), providing strong signal amplification and versatile biosensing performance in aqueous diagnostic applications.

Highlights

- 4-DMAP is a potent alternative to TPrA, generating 180-fold stronger ECL intensities
- It is highly water soluble and chemically stable at room temperature
- 4-DMAP excites oxidized luminophores through a radical process
- The $[Ru(bpy)_3]^{2+}$/4-DMAP system enabled highly sensitive detection of biomarkers

Cho et al., 2025, Cell Reports Physical Science 6, 102864
October 15, 2025
https://doi.org/10.1016/j.xcrp.2025.102864

CellPress

Cell Reports
Physical Science

CellPress
OPEN ACCESS

Article

Discovery of a new coreactant for highly efficient and reliable electrochemiluminescence

Young Kwan Cho,[1,2,10] Sang-Hyun Jeon,[2,10] Jung Yeon Park,[3] Hyunho Kim,[1,4] Beom-Jun Shim,[2] Kyeonghyeon Nam,[5] Simone Swantje Köcher,[6] Haeun Lee,[2] Hyun-Kyung Woo,[1,7] Jay Hoon Park,[8] Yongju Kim,[3] Jong-Seo Kim,[9] Hakho Lee,[1,7,*] and Ik-Soo Shin[2,11,*]

[1]Center for Systems Biology, Massachusetts General Hospital, Harvard Medical School, Boston, MA 02114, USA
[2]Department of Chemistry, Soongsil University, 369 Sangdo-Ro, Dongjak-Gu, Seoul 06978, South Korea
[3]KU-KIST Graduate School of Converging Science and Technology, Korea University, Seoul 02841, Republic of Korea
[4]School of Mechanical Engineering, Korea University, 145 Anam-ro, Seongbuk-gu, Seoul 02841, South Korea
[5]Theory Department, Fritz-Haber-Institut der Max-Planck-Gesellschaft, Faradayweg 4-6, 14195 Berlin, Germany
[6]Institute of Energy and Climate Research (IEK-9), Forschungszentrum Jülich GmbH, Wilhelm-Johnen-Straße, 52425 Jülich, Germany
[7]Department of Radiology, Massachusetts General Hospital, Harvard Medical School, Boston, MA 02115, USA
[8]Department of Plastics Engineering, University of Massachusetts Lowell, Lowell, MA 01854, USA
[9]School of Biological Sciences, Seoul National University, Seoul 08826, South Korea
[10]These authors contributed equally
[11]Lead contact
*Correspondence: hlee@mgh.harvard.edu (H.L.), extant@ssu.ac.kr (I.-S.S.)
https://doi.org/10.1016/j.xcrp.2025.102864

SUMMARY

Using luminophore and coreactant pairs increases light emission in electrochemiluminescence (ECL) reactions, improving the overall sensitivity of ECL assays. The most commonly used coreactant is tri-*n*-propylamine (TPrA) for its capability as a reducing agent. However, TPrA is hydrophobic and readily oxidized, which limits its utility in biosensing. Here, we report the discovery and characterization of the new coreactant 4-(dimethylamino)pyridine (4-DMAP). The compound is highly water soluble and chemically stable under ambient conditions. Most importantly, 4-DMAP generated ECL signals >180 times higher than TPrA in tris(bipyridine)ruthenium(II) $[Ru(bpy)_3]^{2+}$. The 4-DMAP ECL enabled ultra-sensitive and robust immunoassays. For example, the 4-DMAP ECL reliably detected protein markers in extracellular vesicles from the plasma samples of cancer patients. It also achieved >200-fold higher sensitivity than TPrA-ECL did in quantifying neutralizing antibodies against SARS-CoV-2 in human saliva. These findings could lead to exciting new opportunities for using ECL-based sensing in a range of clinical applications.

INTRODUCTION

Electrochemiluminescence (ECL) is a powerful biosensing modality.[1–3] ECL is based on a unique signaling mechanism, chemiluminescence, triggered by an electrochemical potential.[4–6] This turn-on machinery confers competitive advantages, including exceptional sensitivity with a negligible optical background, consistent analytical signal through the spatiotemporal control of chemical reactions, and measurement setups simpler than other assay methods.[7,8] An ECL signal can be generated when radical cations and anions of luminophores (i.e., light-emitting species) interact and annihilate radiatively.[9,10] Alternatively, ECL can be mediated by an added reagent (coreactant) that excites luminophores to induce their light emission.[1,11] This coreactant pathway amplifies light signals while ensuring stable ECL reactions in various media.[12–14] With such merits, the coreactant system has become a core technique in most ECL assays, including commercial ones for clinical diagnostics (e.g., Elecsys by Roche).[15]

The coreactant frequently used in ECL is tri-*n*-propylamine (TPrA), an aliphatic amine.[9,11,16] When electro-oxidized, TPrA becomes a potent reducing agent, efficiently donating electrons to luminophores. TPrA typically pairs with a ruthenium-based luminophore, tris(bipyridine)ruthenium(II) $[Ru(bpy)_3]^{2+}$. This combination is effective in ECL generation and cost effective, thereby widely adopted in bioassays. However, the $[Ru(bpy)_3]^{2+}$./TPrA system has intrinsic drawbacks: (1) hydrophobic TPrA has poor compatibility with biomolecules,[17,18] (2) high doses of TPrA (>100 mM) are typically recommended to generate sufficient ECL signals,[19] and (3) the material is highly toxic (corrosive)[16] and degrades over time through spontaneous reaction with oxygen.[20] These limitations prompted intensive investigations to search for TPrA replacements, yet the results are unsatisfactory. For instance, other aliphatic-amine forms, such as 2-(dibutylamino)ethanol[16] and N-dipropyl isobutyl amine,[11] have shown higher ECL signals than TPrA, albeit their water solubility is comparable to that of TPrA. Conversely, hydrophilic coreactants (e.g., doped carbon nanodots) were found to be inferior to TPrA in ECL efficiency.[21,22] As a promising TPrA replacement, 2,2-bis(hydroxymethyl)-2,2′,2′′-nitrilotriethanol has been demonstrated, but its application has been largely

confined to oxide-coated electrodes.[23] To further advance ECL-based biosensing, it thus remains an unmet need to establish new coreactants that are hydrophilic, efficient at low doses, chemically robust, and compatible with common electrodes.

Here, we report the discovery of a new ECL coreactant surpassing TPrA. Instead of relying on an aliphatic amine structure, we explored the use of aromatic rings modified with amine functional groups. We specifically chose pyridine as the base structure for its water solubility and subsequently evaluated a panel of pyridine derivatives for their ECL generation with $[Ru(bpy)_3]^{2+}$ luminophore. This screening identified 4-(dimethylamino)pyridine (4-DMAP) as the most efficient ECL coreactant. Remarkably, using 4-DMAP resulted in an ECL intensity >180-fold higher than that of TPrA. Ensuing mechanism studies revealed a three-step process that renders 4-DMAP a radical reductant to excite the oxidized luminophore ($[Ru(bpy)_3]^{3+}$) for ECL generation. Due to their excellent ECL efficiency, the 4-DMAP-based bioassays outperformed the TPrA system. The $[Ru(bpy)_3]^{2+}$/4-DMAP ECL achieved >200-fold higher sensitivity in immunoassays at a low coreactant concentration (10 mM). Moreover, the 4-DMAP solution was chemically stable under ambient conditions and can be in powder form for long-term storage. These findings highlight the potential of 4-DMAP to expand the practical value of ECL-based biosensing.

RESULTS

Screening ECL coreactant candidates

The initial screening started with pyridine and its derivatives (Figure 1A): 4-methoxypyridine (4-MP), 4-(methylamino)pyridine (4-MAP), 4-aminopyridine (4-AP), 2-(dimethylamino)pyridine (2-DMAP), and 4-DMAP. We excluded 3-DMAP due to its limited commercial availability and the complexities involved in synthesis.[24,25] We first characterized the electrochemical behavior of these compounds via cyclic voltammetry (Figures 1B, S1, and S2). To be eligible as a coreactant, the compound is required to undergo electrochemical oxidation within the potential range that permits subsequent ECL reactions while avoiding direct water oxidation.[9,26] Pyridine compounds with amine branches (i.e., 4-MAP, 4-AP, 2-DMAP, and 4-DMAP) satisfied these criteria, apparently due to amine oxidation in these compounds.

We next assessed ECL generation with the coreactant candidates. Each compound was mixed with $[Ru(bpy)_3]^{2+}$ (1 μM), and the mixture was subject to ECL measurements (methods). The experiments revealed substantial ECL signals only with 2-DMAP and 4-DMAP (Figures 1C and S3). A tertiary amine group was present in both compounds, indicating its dominant role in ECL generation. This result is consistent with previous findings[16,27]: oxidized tertiary amines were essential for producing ECL signals when alkylamines (e.g., TPrA) were used as coreactants.

Interestingly, 4-DMAP produced much higher (>23 times) ECL signals than 2-DMAP. Molecular simulations based on density functional theory (DFT) revealed that 4-DMAP undergoes considerable changes in the highest occupied molecular orbital (HOMO) after oxidation (Figure 1D). Specifically, the oxidized 4-DMAP became electron poor in its tertiary amine branch, which would lead to rapid deprotonation of the methyl group to form a nucleophilic (or reductive) radical intermediate as a conjugation base. This condition would facilitate the electron exchange reaction with luminophores, the most critical step in ECL generation. In contrast, the dimethylamino group in 2-DMAP maintained a large HOMO lobe after oxidation, which made the deprotonation unfavorable. Further calculation of the pK_a values aligned with this reasoning (methods). The estimated pK_a values were 7.8 for cationic 4-DMAP and 9.8 for cationic 2-DMAP (Figure S4). Based on this screening, we selected 4-DMAP as the final coreactant candidate.

ECL mechanism with 4-DMAP coreactant

Our next focus was to investigate 4-DMAP's role in ECL generation. Drawing from electrochemical data and molecular simulation, we postulated the following mechanism (Figure 2A). First, both $[Ru(bpy)_3]^{2+}$ and 4-DMAP are oxidized on the working electrode surface (see Figure S5 for electrochemical characterization).

$$4-\mathrm{DMAP}\ (\mathbf{1}) \longrightarrow 4-\mathrm{DMAP}^{\cdot+}\ (\mathbf{2}) + e^- \quad \text{at } E_{1/2}(\mathrm{ox}) = 0.81\ \mathrm{V}\ (\mathrm{vs.\ Ag/Ag^+}) \qquad \text{(Equation 1)}$$

$$\left[Ru(bpy)_3\right]^{2+} \longrightarrow \left[Ru(bpy)_3\right]^{3+} + e^- \quad \text{at } E_{1/2}(\mathrm{ox}) = 0.95\ \mathrm{V}\ (\mathrm{vs.\ Ag/Ag^+}) \qquad \text{(Equation 2)}$$

The cationic 4-DMAP$^{\cdot+}$ rapidly loses a proton, forming a radical reductant, 4-DMAP·.

$$4-\mathrm{DMAP}^{\cdot+}\ (\mathbf{2}) \longrightarrow 4-\mathrm{DMAP}\cdot + H^+. \qquad \text{(Equation 3)}$$

This radical then donates an electron to $[Ru(bpy)_3]^{3+}$. This exergonic reaction excites the luminophore to $[Ru(bpy)_3]^{2+*}$ and also produces an intermediate product (IP; 3) in the form of the iminium cation.

$$\left[Ru(bpy)_3\right]^{3+} + 4-\mathrm{DMAP}\cdot \rightarrow \left[Ru(bpy)_3\right]^{2+*} + \mathrm{IP}(\mathbf{3}). \qquad \text{(Equation 4)}$$

Finally, the excited luminophore emits visible light (wavelength, 610 nm) and returns to its initial state $[Ru(bpy)_3]^{2+}$ for reuse.

$$\left[Ru(bpy)_3\right]^{2+*} \longrightarrow \left[Ru(bpy)_3\right]^{2+} + h\nu. \qquad \text{(Equation 5)}$$

Meanwhile, the IP (3) undergoes hydrolysis that breaks the C-N bond in the amine branch. This results in the formation of 4-MAP and formaldehyde.

$$\mathrm{IP}\ (\mathbf{3}) + H_2O \longrightarrow 4-\mathrm{MAP}\ (\mathbf{4}) + CH_2O + H_3O^+. \qquad \text{(Equation 6)}$$

To test the proposed mechanism, we performed a series of analytical measurements (see methods) on the mixture of $[Ru(bpy)_3]^{2+}$ and 4-DMAP immediately after ECL reaction. High-resolution electrospray ionization-mass spectrometry detected monoisotopic ion peaks corresponding to the molecules in the proposed mechanism (Figure 2B): m/z = 123.092 (relative error, 2.64 ppm) for the adduct [4-DMAP + H]$^+$ of the residual 4-DMAP (1); m/z = 121.076 (2.68 ppm) for the IP (3); and

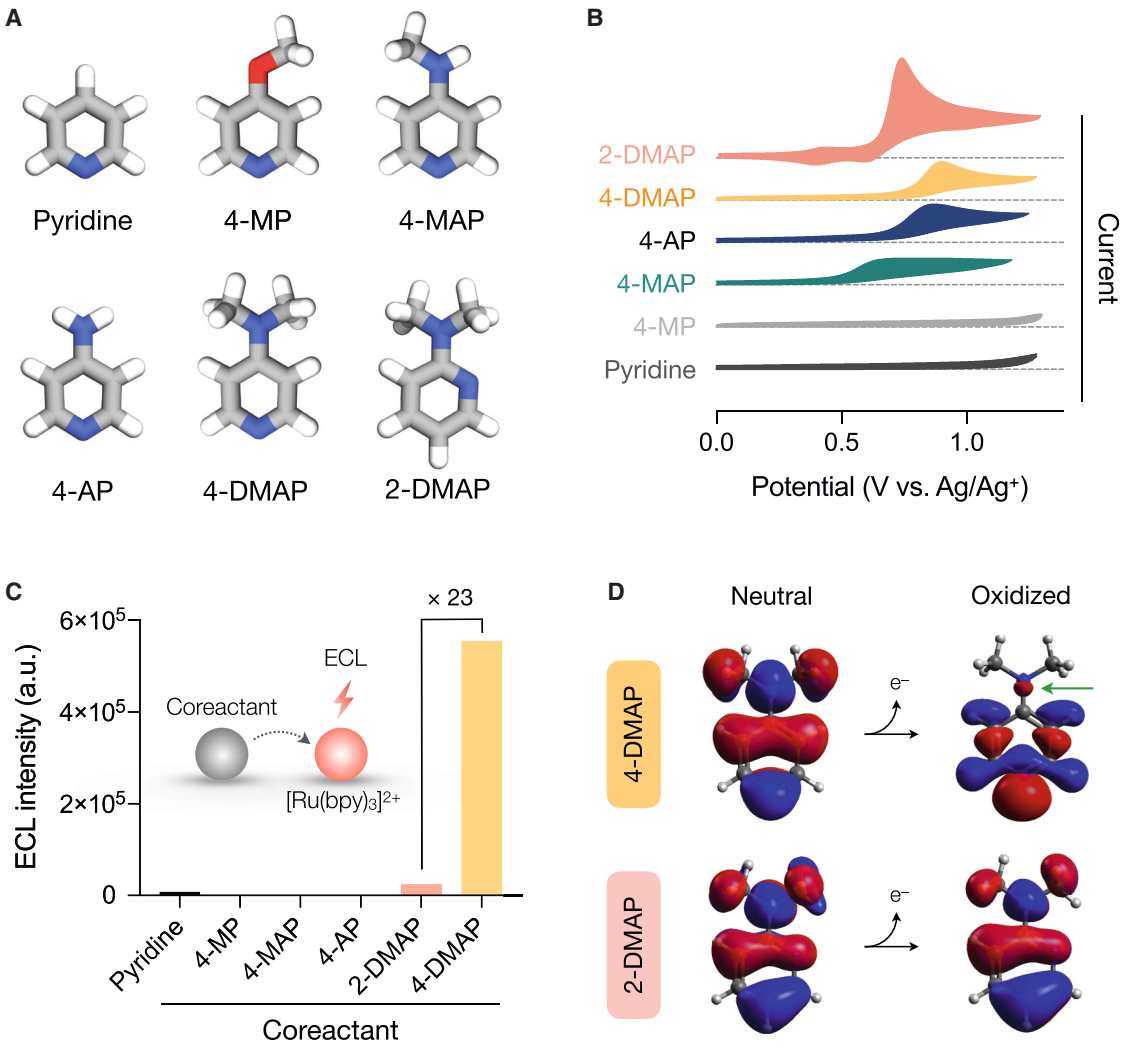

Figure 1. ECL coreactant candidates

(A) Chemical structure of six candidate compounds: pyridine, 4-methoxypyridine (4-MP), 4-methylaminopyridine (4-MAP), 4-aminopyridine (4-AP), 2-(dimethylamino)pyridine (2-DMAP), and 4-(dimethylamino)pyridine (4-DMAP). All candidates have a pyridine structure and dissolve well in aqueous buffers.

(B) The candidate compounds were dissolved in acetonitrile solution to avoid signal interference from the solvent oxidation, and then cyclic voltammograms were measured. Four candidates (2-DMAP, 4-DMAP, 4-AP, and 4-MAP) exhibited electrochemical oxidation at potentials below 1.0 V (vs. Ag/Ag^+). See Figures S1 and S2 for individual voltammograms. The potential range was from 0 to 1.3 V at the scan rate of 100 mV/s

(C) The coreactant candidates (10 mM) were used with luminophore $[Ru(bpy)_3]^{2+}$ (1 μM) for the ECL reaction in aqueous buffer (pH 7.4, 0.2 M phosphate). Both 2-DMAP and 4-DMAP generated ECL signals, with the signal from 4-DMAP substantially stronger than that from 2-DMAP.

(D) Highest occupied molecular orbital (HOMO) calculation. (Top) HOMO of 4-DMAP and its oxidized cation; (bottom) HOMO of 2-DMAP and its oxidized cation. In 4-DMAP, the lobe size of the dimethylamino group markedly decreases after oxidation (green arrow); this state favors the deprotonation of the methyl group to form a conjugated base. In 2-DMAP, the dimethylamino group maintained HOMO localization, making the deprotonation unfavorable.

m/z = 109.076 (1.15 ppm) for the adduct $[4\text{-MAP} + H]^+$ of 4-MAP (4).

We further investigated the electronic state of 4-DMAP using electron paramagnetic resonance (EPR). This technique allowed us to determine the oxidation position in the transient $4\text{-DMAP}^{\cdot+}$ cation (2). The simulated spectrum of the oxidized nitrogen atom adjacent to the tertiary amine matched the measured EPR spectrum (Figures 2C and S6) in both position and the number of resonance peaks. This result supports the presence of electron-poor radicals, as suggested in Figure 1D.

4-DMAP surpasses TPrA in ECL generation

We benchmarked 4-DMAP against TPrA for the ECL performance. The test setup measured light emission from $[Ru(bpy)_3]^{2+}$ (1 μM) via cyclic voltammetric and pulsed ECL measurements (Figure S7) on screen-printed Au electrodes.[25,26] Applying the pulsed ECL method, we further monitored maximum signal intensities at varying coreactant concentrations (Figure 3A). Overall, the 4-DMAP coreactant system generated a markedly higher ECL signal than the TPrA system; the increase was up to 180-fold at the optimal coreactant concentration of 10 mM. Above this

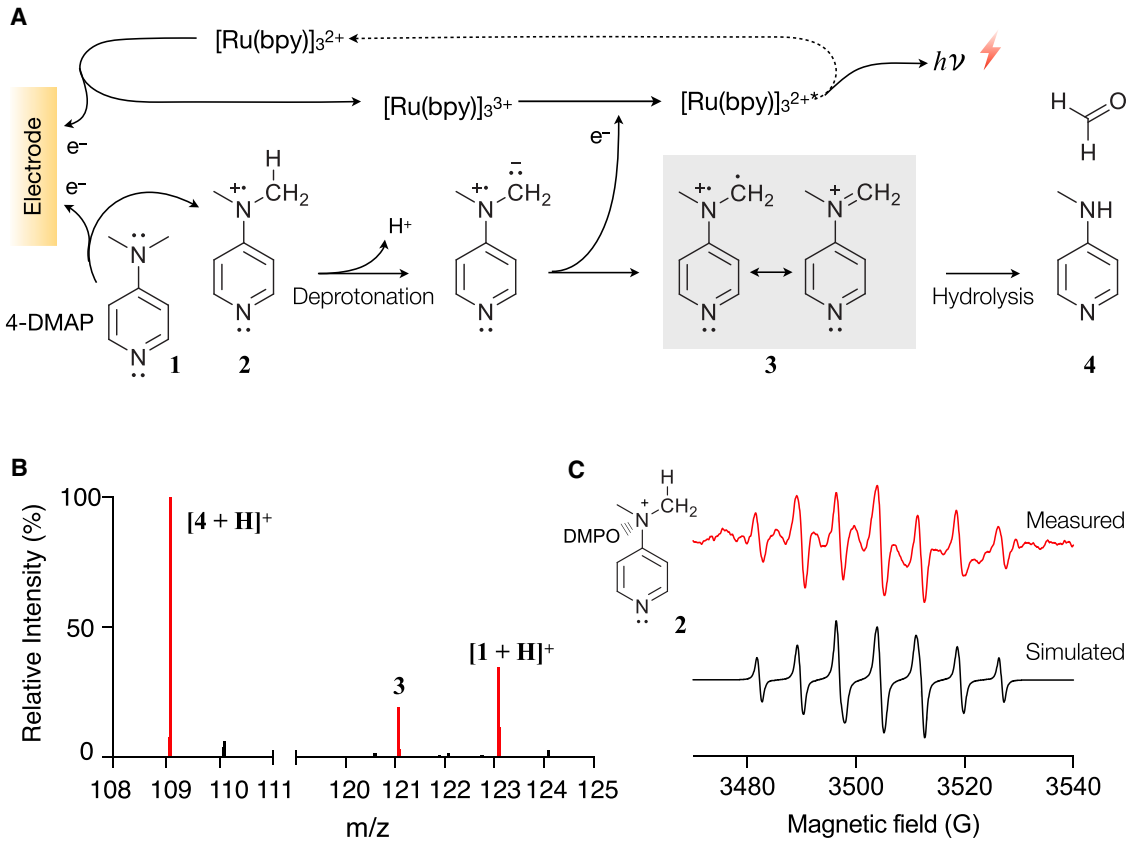

Figure 2. ECL mechanism with 4-DMAP

(A) Proposed ECL cycle. Both 4-DMAP (1) and $[Ru(bpy)_3]^{2+}$ are oxidized on an anode. The cationic 4-DMAP (2), with an unpaired electron at the amino N, rapidly deprotonates into a nucleophilic 4-DMAP radical. This energetic radical then donates an electron to excite $[Ru(bpy)_3]^{3+}$, becomes an intermediate product (3), and eventually degrades into 4-MAP (4). The excited $[Ru(bpy)_3]^{2+*}$ emits a photon and returns to its ground state.

(B) Mass spectrometry of a post-ECL mixture detected a trace of the original 4-DMAP (1) and its deprotonated and a single electron ejected resonance intermediate form (3). The major component was the final product 4-MAP (4).

(C) Electron paramagnetic resonance (EPR) analysis detected the presence of cationic 4-DMAP radicals (2). The number and location of resonance peaks matched between the measured data (red line) and the simulated spectrum (black line).

concentration, the ECL intensity gradually decreased, which could be attributed to the "father-son" process.[28] The proton generated from 4-DMAP$^{\cdot+}$ (2) can react with neutral 4-DMAP (1), generating non-electroactive protonated species (4-DMAPH$^+$). This reaction effectively reduces the concentration of electroactive species (the neutral 4-DMAP) within the electrode diffusion layer, leading to a decrease in the ECL signal.

For a more rigorous comparison, we further assessed the relative ECL efficiency. Both TPrA and 4-DMAP exist predominantly in their conjugate acid forms (TPrAH$^+$ and 4-DMAPH$^+$) in buffered aqueous solutions (pH 7.4). Utilizing the Henderson-Hasselbalch equation and pK_a values of 10.4 for TPrAH$^+$ and 9.6 for 4-DMAPH$^+$, the concentrations of the neutral base forms are given as [TPrA] = 0.001·[TPrAH$^+$] and [4-DMAP] = 0.006·[4-DMAPH$^+$]. Therefore, in the experiments employing 10 mM input coreactants, the concentrations of active species participating in ECL reactions would be 0.01 mM for TPrA and 0.06 mM for 4-DMAP. The relative ECL efficiency was then estimated as $\Phi_{ECL,4\text{-}DMAP}/\Phi_{ECL,TPrA} = (I_{4\text{-}DMAP}/[4\text{-DMAP}])/(I_{TPrA}/[TPrA])$, where $\Phi_{ECL,x}$ represents the ECL efficiency for coreactant x, and I_x denotes the corresponding signal intensity. Substituting the experimentally measured signal intensity ratio ($I_{4\text{-}DMAP}/I_{TPrA}$ = 183) and the concentration ratio ([4-DMAP]/[TPrA] = 6) yields a relative ECL efficiency of 30.5.

The 4-DMAP system further demonstrated superior signal reliability. When ECL was triggered by a train of potential pulses (Figure 3B), the 4-DMAP system reported consistent signals, with a coefficient of variation (CV) of 3% for the initial ten ECL peaks. In contrast, the TPrA system showed a gradual signal increase after the first ECL peak, leading to larger CV values (19.4% for the initial ten ECL peaks). The signal stability was also confirmed in a prolongated emission, wherein a constant potential was applied for 50 s to generate a continuous ECL (Figure S8). We observed that ECL with 10 mM 4-DMAP surpassed that of both 10 and 180 mM TPrA.

With its strong and robust ECL signal, the 4-DMAP system achieved excellent analytical sensitivity (Figure 3C). We measured ECL signals at varying $[Ru(bpy)_3]^{2+}$ concentrations while keeping the coreactant concentration constant (10 mM). The estimated limits of detection (LODs) were 4.0 pM $[Ru(bpy)_3]^{2}$

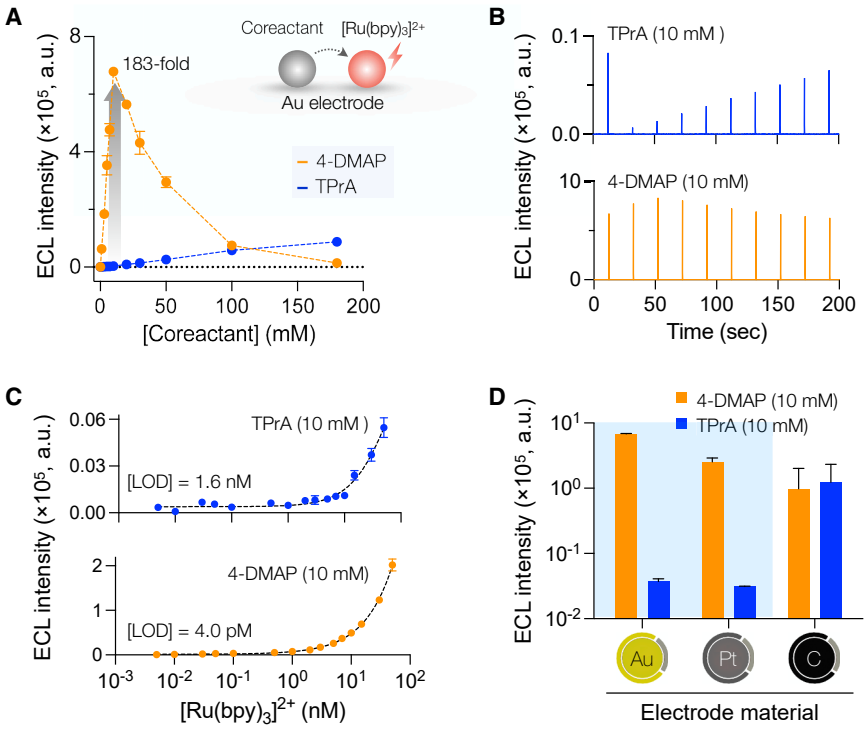

Figure 3. ECL performance of 4-DMAP

(A) ECL intensity from $[Ru(bpy)_3]^{2+}$ (1 μM) was compared at varying coreactant concentrations. The 4-DMAP system generated over 180-fold higher signal than TPrA. Coreactant solutions were prepared by dissolving each compound in 0.2 M phosphate buffer, with the final pH adjusted to 7.4. ECL signals were generated by applying potential pulses (height, 1.2 V; width, 0.1 s; period, 20 s; and repetition, 10) on screen-printed Au electrodes. ECL values from the 6th to 10th pulses were averaged. Data are displayed as mean ± SD from technical triplicates.

(B) Raw ECL intensities from pulsed potential measurements. The signals from the 4-DMAP system were consistent across the pulse train, whereas the TPrA system displayed a fluctuating pattern (an initial peak, collapse, and slow recovery). The pulse profiles were the same as in (A).

(C) Analytical sensitivity was assessed by changing $[Ru(bpy)_3]^{2+}$ concentrations. With its robust ECL signal, the 4-DMAP assay achieved about a 400-fold lower detection limit than the TPrA assay. Data are displayed as mean ± SD from technical triplicates. The ECL reaction conditions were the same as in (b). ECL values from 6th to 10th pulses were averaged. Data are displayed as mean ± SD from technical triplicates.

(D) When used with metal electrodes (Au, Pt), the 4-DMAP system produced higher ECL signals than TPrA. With a carbon (C) electrode, the 4-DMAP ECL signal was slightly reduced (40% of the TPrA ECL intensity). Data are displayed as mean ± SD from technical triplicates. The ECL reaction conditions were the same as in (B) and (C).

with 4-DMAP and 1.6 nM with TPrA. The LOD improvement (~400-fold) was of the same magnitude as the signal enhancement. We also tested the compatibility of 4-DMAP with various electrode materials (Figure 3D). Using noble metal (Au and Pt) electrodes in combination with 4-DMAP resulted in improved ECL signals. This enhancement is likely due to the hydrophilic nature of both the 4-DMAP and the electrodes, which can facilitate 4-DMAP's adsorption to the electrode surface and subsequent electron transfer.[17] In contrast, hydrophobic carbon electrodes would impede this process, leading to the observed lower ECL signal relative to TPrA (40% lower signal).

Advantages of 4-DMAP coreactant

Besides producing high ECL signals, 4-DMAP had practical advantages. The raw material is available as a solid powder and can be stored at ambient conditions, whereas TPrA comes as a liquid (melting point: −93°C) and needs to be stored under inert gas.[17,18] In addition, 4-DMAP was highly soluble in an aqueous buffer (>1,000 mM in 0.2 M phosphate) and remained stable (Figure 4A, bottom); the compound maintained its integrity after more than 6 months of storage at room temperature. On the other hand, TPrA gradually degraded over time, likely through oxidation by dissolved oxygens (Figure 4A, top). With its superb chemical stability, 4-DMAP enabled reproducible ECL assays, contrasting with TPrA (Figure 4B). Using the same 4-DMAP solution over a month, we obtained consistent ECL signals with a CV value of 3.0%. With TPrA, the CV value was close to 20%.

4-DMAP was also compatible with flow cell-type assays that are often used in commercial assay systems (e.g., cobas, Roche). To emulate such assays, we assembled a prototype device by attaching a fluidic cell on top of a planar electrode (Figures 4C and S9). Once ECL reagents were delivered over the electrode by a syringe pump, we applied a potential and imaged the electrode using a camera. 4-DMAP consistently generated higher ECL signals than TPrA (Figure 4D), which was in line with the results obtained without using flow cells. No hardware modifications were necessary to use 4-DMAP, demonstrating its effectiveness as a drop-in substitute for TPrA in existing systems.

ECL bioassays using 4-DMAP as a coreactant

We evaluated the 4-DMAP system in ECL biosensing. We adopted the bead-based assay wherein molecular targets were first captured on magnetic beads conjugated with affinity ligands (e.g., proteins or antibodies) and further labeled with $[Ru(bpy)_3]^{2+}$ (Figure 5A). The bead complexes were then combined with coreactant solutions and placed on Au electrodes. We first optimized bioassay conditions. Among the different buffers tested, phosphate buffer yielded the highest ECL signal (Figure S10A). Buffer pH also affected the ECL intensity (Figure S10B). The signal peaked around neutral pH (6–7); we decided to use neutral (pH 7.4) phosphate buffer as our working ECL solution for 4-DMAP, which provided a favorable bioassay condition.

We proceeded to characterize the performance of 4-DMAP in the bead-based ECL. In this assay configuration, most luminophores ($[Ru(bpy)_3]^{2+}$) are rarely oxidized by an electrode due to their spatial separation from the electrode surface. ECL generation would rather follow the heterogeneous mechanism

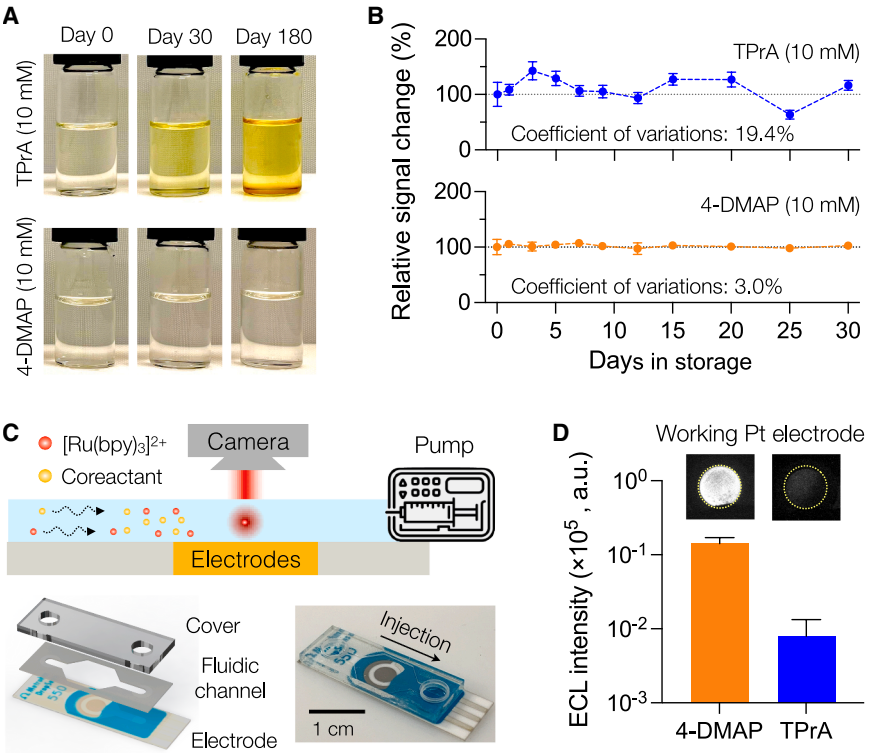

Figure 4. Practical advantages of 4-DMAP

(A) Material stability. 4-DMAP (10 mM) and TPrA (10 mM) solutions were prepared by dissolving each compound in 0.2 M phosphate buffer (pH 7.4). TPrA solution gradually discolored under the ambient storage condition (top), whereas 4-DMAP showed no apparent changes (bottom).

(B) Coreactant solutions in (A) were stored in ambient conditions and monitored for quality. 4-DMAP yielded consistent ECL signals, with a CV of 3.0%. In contrast, the CV value was nearly 20% with TPrA. ECL signals were measured via pulsed potential measurements (pulse height, 1.2 V; pulse width, 0.1 s; and pulse period, 20 s). The luminophore ($[Ru(bpy)_3]^{2+}$) concentration was 1 μM, and screen-printed Au electrodes were used. Data are displayed as mean ± SD from technical triplicates.

(C) A prototype system was configured for flow-cell-type ECL assays (top). The ECL cell had a fluidic chamber on top of a Pt-planar electrode (bottom). A syringe pump injected ECL reagents into the ECL cell, and a camera imaged the electrode for ECL detection.

(D) The 4-DMAP system produced higher ECL signals than TPrA in the flow-cell assay. Coreactant solutions were 4-DMAP (10 mM) and TPrA (10 mM) in 0.2 M phosphate buffer (pH 7.4), and the luminophore was $[Ru(bpy)_3]^{2+}$ (1 μM). The working electrode was screen-printed Pt, and a constant potential of 1.2 V (vs. AgQRE) was applied for the ECL reaction (acquisition time, 60 s). Data are displayed as mean ± SD from technical duplicates.

(Figure S11A), similar to that proposed for bead-based ECL involving TPrA.[27] The process can be described as follows: (1) both cationic radicals of 4-DMAP (4-DMAP·$^+$) and neutral free radicals (4-DMAP·) are generated near the electrode surface and diffuse toward the beads; (2) the neutral reductive radicals (4-DMAP·) reduce $[Ru(bpy)_3]^{2+}$ to $[Ru(bpy)_3]^{+}$; (3) the cationic radicals (4-DMAP·$^+$) further oxidize $[Ru(bpy)_3]^{+}$, resulting in the excited state $[Ru(bpy)_3]^{2+*}$; and (4) $[Ru(bpy)_3]^{2+*}$ emits light before returning to its ground state $[Ru(bpy)_3]^{2+}$ for recycling.

Under this process, ECL signals are anticipated to diminish rapidly with increasing distance between the electrode and $[Ru(bpy)_3]^{2+}$. The cationic radicals (4-DMAP·$^+$) can be depleted before reaching $[Ru(bpy)_3]^{2+}$ as a result of their spontaneous conversion into 4-DMAP·. To validate this reasoning, we used differently sized beads and assessed the ECL efficiency, following the recently reported ECL imaging method (see supplemental note).[11] Our findings indeed demonstrated a reduction in ECL efficiency with larger beads (Figure 5B); consistent findings have been reported for other coreactants.[11,29] Based on these results, the lifetime of 4-DMAP·$^+$ was estimated to be in the order of 10^{-3} s (see Supplementary Note). Conversely, the typical diffusional distance of 4-DMAP·$^+$ would be 2.7 μm (supplemental note). Furthermore, no ECL signal was observed in the absence of 4-DMAP, underscoring the requirement of 4-DMAP oxidation in the bead-based ECL (Figure S11B). In a direct comparison with TPrA, 4-DMAP (10 mM) consistently generated stronger ECL signals than both 10 and 180 mM TPrA (Figure S12), which confirmed 4-DMAP's suitability as a superior coreactant for bead-based assays.

As a pilot bioassay, we applied the 4-DMAP ECL to detect extracellular vesicles (EVs) in human blood. EVs are nanoscale particles secreted by cells.[30] They carry molecular cargoes from tumor cells and readily circulate in easily accessible bodily fluids. Analyzing EVs can thus have implications for cancer diagnosis through minimally invasive liquid biopsy.[31,32] We captured EVs on magnetic beads conjugated with antibodies against CD63, a common EV surface marker[33]; these EVs were then labeled with probe antibodies against cancer biomarkers. EV-titration experiments reaffirmed the superior sensitivity of the 4-DMAP ECL assay (Figure 5C). With EVs derived from colorectal cancer (CRC) cells (SW620; Figure S13), the 4-DMAP ECL achieved the detection limit of about 1.5×10^4 EVs/mL. Next, we applied the 4-DMAP assay to analyze EVs in clinical plasma samples (18 CRC patients and 18 non-cancer controls; Table S1). We profiled EVs for key CRC markers, EpCAM and EGFR, that were identified in our previous study.[31] The 4-DMAP assay produced robust molecular profiles (Figure 5D), which led to high accuracy (sensitivity, 0.94; specificity, 0.94) in CRC diagnostics (Figure S14).

We also configured the 4-DMAP assay to detect antibodies in bodily fluids. We immunomagnetically captured IgG antibodies labeled with luminophores (see methods for details). The 4-DMAP ECL assay markedly outperformed the TPrA assay (Figure 5E) and achieved the limit of detection of 42 fg/mL [IgG], which was 260-fold lower than that of the TPrA assay (11 pg/mL [IgG]). We next tested the 4-DMAP ECL assay in human specimens (Table S2), specifically targeting neutralizing antibodies (nAbs) against severe acute respiratory syndrome

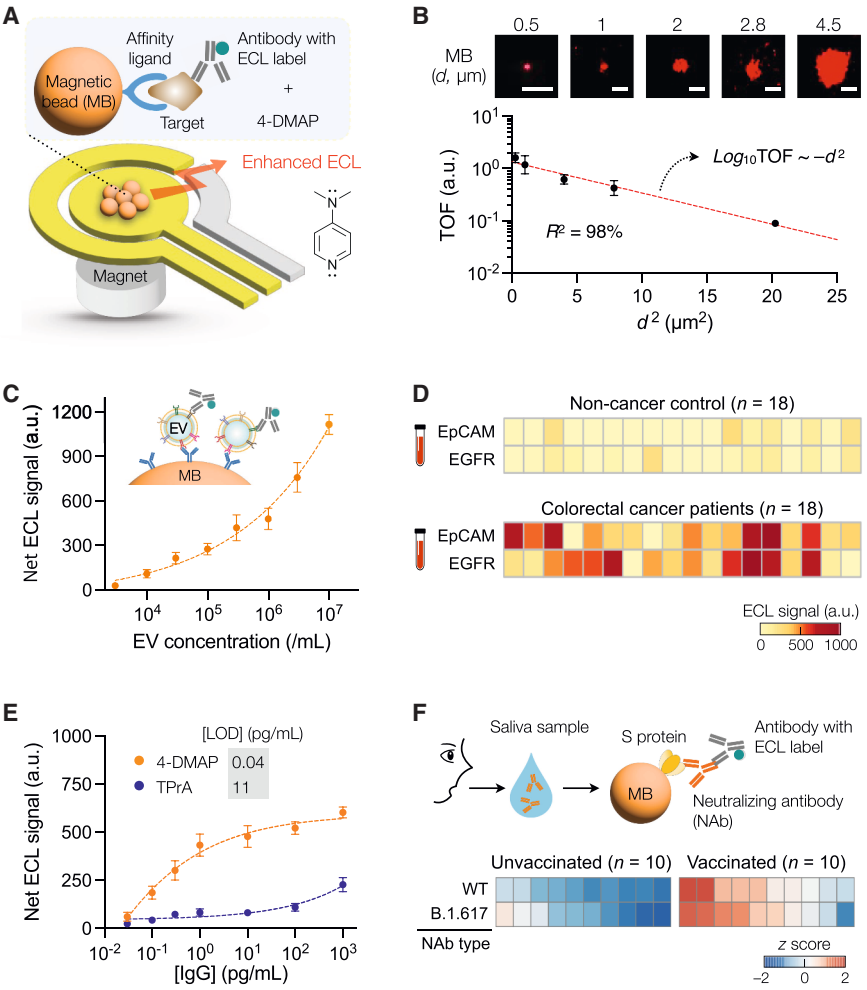

Figure 5. Bead-based ECL bioassays

(A) Molecular targets were captured on magnetic beads (MBs) conjugated with affinity ligands and further labeled with luminophore through probe antibodies. The bead complexes were mixed with coreactants and placed on Au electrodes for ECL measurements.

(B) Bead-based ECL experiments were conducted using MBs of different diameters (d). ECL efficiency was compared by estimating the turnover frequency (TOF), which is proportional to the number of photons produced per unit of time for each luminophore. TOF decreased as the diameter increased, with $Log_{10}TOF$ showing a linear dependency on d^2. The inset shows micrographs of MBs during the ECL reaction. Scale bar, 1 μm. Applied potential, 1.2 V (vs. AgQRE); image integration, 50 s. The coreactant was 10 mM 4-DMAP in 0.2 M phosphate buffer (pH 7.4). Each data point represents mean ECL intensity ± SD from nine beads.

(C) Extracellular vesicles (EVs) were detected by the 4-DMAP ECL assay. EVs were captured on CD63-specific MBs and further immuno-labeled for EpCAM. The observed detection limit was 1.5×10^4 EVs/mL. The coreactant solution was 4-DMAP (10 mM) in 0.2 M phosphate buffer (pH 7.4), and the pulsed ECL measurements as in (B) were conducted. Data are displayed as mean ± SD from technical triplicates.

(D) The 4-DMAP assay was used to analyze EVs in clinical plasma samples (18 colorectal cancer patients and 18 non-cancer controls). Profiling EVs for EpCAM and EGFR markers enabled high accuracy in cancer diagnostics. The same ECL experimental conditions as in (C) were applied. The heatmap shows mean values from duplicate measurements.

(E) ECL assay was applied to detect IgG antibodies. The 4-DMAP ECL assay achieved a detection limit of 42 fg/mL [IgG], which was 260-fold lower than that of the TPrA assay (11 pg/mL [IgG]). Coreactant solutions were prepared by dissolving 4-DMAP (10 mM) or TPrA (10 mM) in 0.2 M phosphate buffer (pH 7.4). Pulsed ECL measurements were performed as in (C). Data are displayed as mean ± SD from technical triplicates.

(F) The IgG assay was extended to detect neutralizing antibodies (nAbs) against SARS-CoV-2, both for wild-type (WT) virus and B.1.617 (delta) variants. The assay revealed the presence of both nAb types in the salivary samples of vaccinated individuals. The same ECL experimental conditions as in (E) were applied. The heatmap shows mean values from duplicate measurements.

coronavirus 2 (SARS-CoV-2). Magnetic beads were conjugated with viral antigens (S proteins) either from the SARS-CoV-2 wild type (wt) or the B.1.617 (delta) variant. Using the prepared beads, we analyzed saliva samples from SARS-CoV-2-vaccinated individuals (n = 10). As a negative control, we used saliva samples from individuals (n = 10) before vaccination and without a prior history of infection. The 4-DMAP assay detected nAbs against both WT and delta SARS-CoV-2 in all vaccinated individuals (Figure 5F), confirming previous studies that reported the presence of nAbs in saliva.[34,35]

DISCUSSION

We identified 4-DMAP as a promising ECL coreactant with appealing properties. The compound is hydrophilic, chemically stable in air, and can be stored as a solid powder. Notably, it enhanced $[Ru(bpy)_3]^{2+}$ ECL signals by over 180-fold compared to TPrA, substantially empowering ECL-based biosensing. When adopted in bioassays, the 4-DMAP system demonstrated outstanding analytical performances. It yielded reproducible and robust ECL signals, consistently achieving sensitivity approximately two orders of magnitude higher than TPrA-based ECL assays. In our pilot clinical studies, we could reliably detect various biological targets (e.g., antibodies and EVs) in different bodily fluids, such as saliva and plasma, which further proved the effectiveness of the 4-DMAP assay.

We investigated 4-DMAP's working mechanism through comprehensive chemical analyses. Molecular simulations based on DFT calculations indicated that 4-DMAP could undergo sacrificial reactions, wherein the dimethylamino group in the radical cation loses a proton (H^+) after electrochemical oxidation and becomes primed to excite luminophores. The DFT calculation further highlighted the importance of the amine's location in the pyridine.[36,37] In 2-DMAP, which has an amine group attached

to the 2-position of the pyridine, the electron from the pyridine nitrogen could be shared with an oxidized amine group, which apparently hinders the deprotonation process. Results from our experiments supported such reasoning. Mass spectrometry detected chemical species whose masses corresponded to the expected reaction intermediates and the 4-DMAP byproducts. EPR analysis further confirmed the electrochemical oxidation of the nitrogen atom in the tertiary amine group. Based on these observations, we concluded that 4-DMAP follows the coreactant ECL mechanism similar to that of TPrA. However, in the solution used (0.2 M phosphate buffer), 4-DMAP demonstrated higher solubility (>1,000 mM) than TPrA (~331 mM; Figure S15), which is likely to contribute to the increased availability of 4-DMAP for reaction with luminophores.

We envision future research to broaden the scope of the current study. First, we need to further elucidate the underlying 4-DMAP ECL mechanism. For this task, we may employ electrochemistry-mass spectrometry (EC/MS) to detect short-lived radicals and intermediates. This dynamic information will refine the current 4-DMAP ECL pathway and potentially lead to more efficient use of 4-DMAP. Applying spatially resolved ECL imaging would also produce insights for optimizing bead-based bioassays. Second, we can explore 4-DMAP's compatibility with other luminophores. For instance, acridinium or iridium(III) complexes are also regularly paired with TPrA in coreactant ECL. Conceivably, using 4-DMAP instead may amplify ECL signals and provide better chemical stability. Furthermore, expanding compatible luminophores may enable 4-DMAP assays that can detect multiple molecular targets simultaneously through ECL-wavelength multiplexing. Third, we may use 4-DMAP as a direct replacement for TPrA in ECL microscopy. 4-DMAP is expected to facilitate such applications for its hydrophilic nature and ability to generate strong ECL signals at low concentrations. Significantly, 4-DMAP exhibited no acute cytotoxicity at concentrations up to 10 mM, which was the optimal dose for its ECL applications (Figure S16). However, a further assessment is necessary to ascertain the biocompatibility of the overall ECL reaction within cellular environments. Fourth, we can develop an automated, high-throughput ECL assay system. Here, 4-DMAP's practical merits will streamline the system design. A reservoir could be installed to store the coreactant solution without risk of degradation. The fluidic handling would be straightforward because assay processes (e.g., reagent dispensing, mixing, washing) can be readily carried out in an aqueous buffer. Moreover, the strong ECL signal by 4-DMAP will allow us to scale down many reaction cells into a small array for high-throughput assays. This will, in turn, simplify the detection optics as a camera can image the entire array without requiring mechanical scanning. With these advances, the 4-DMAP system has the potential to improve upon current ECL assays and serve as a new approach in bioanalytical technologies.

METHODS

Materials

Tris(2,2′-bipyridyl)dichlororuthenium(II) hexahydrate (99.95% trace metals basis), tris(2,2′-bipyridine)ruthenium(II) hexafluorophosphate (97%), 4,4′-dipyridyl (98%), 4-aminopyridine (AP, ≥99%), 4-(methylamino)pyridine (4-MAP, 98%), 4-DMAP (≥99%), 2,2′-bipyridyl (≥99%), potassium phosphate monobasic (≥99%), potassium phosphate dibasic (≥98%), pyridine (≥99%), 5,5-dimethyl-pyrroline N-oxide (DMPO, ≥98%), Amicon centrifugal filter (3 kDa, 0.5 mL), TPrA, and tetrabutylammonium hexafluorophosphate ($TBAPF_6$) were purchased from Sigma-Aldrich. 4-methoxypyridine (≥98%) and 2-DMAP were purchased from Tokyo Chemical Industry. Bis(2,2′-bipyridine)-4′-methyl-4-carboxybipyridine-ruthenium N-succinimidyl ester-bis(hexafluorophosphate ($Ru(bpy)_2$(mcbpy-*O*-Su-ester)$(PF_6)_2$) was purchased from Abcam. Table S3 lists information on antibodies and proteins.

Electrochemical measurements

Cyclic voltammetry was conducted using an SP-200 potentiostat (Biologic) on the 10 mM 4-DMAP or alternative coreactant candidates in an acetonitrile solution (0.1 M $TBAPF_6$). The potential was scanned between 0.0 and 1.3 V at the rate of 100 mV/s. We used a three-electrode system: glassy carbon working electrode, Pt-wire counter electrode, and Ag/Ag^+ reference electrode. Prior to the cyclic voltammetry measurements, the solutions were vigorously degassed with high-purity nitrogen. Table S4 provides a summary of the experimental conditions for electrochemical measurements in this study.

ECL measurements

We prepared coreactant solutions by dissolving the candidate chemicals in 0.2 M phosphate buffer, which initially had a pH of 7.4. For 4-DMAP (10 mM) and TPrA (10 mM), the prepared solutions exhibited less than a 2% change in pH, with 4-DMAP at a pH of 7.54 and TPrA at a pH of 7.52. Subsequently, the coreactant solution was mixed with $[Ru(bpy)_3]^{2+}$ (1 μM) and deposited onto a screen-printed electrode. For pulsed ECL measurements, we applied a repeated pulse (1.2 V and 0.1-s duration) every 20 s and measured ECL signals. For cyclic voltammetry application, we scanned the potential between 0.0 and 1.6 V at the rate of 100 mV/s. Unless specified otherwise, ECL measurements were carried out using ECL Station 201A (ELIPS Diagnostics, Seoul, South Korea) equipped with a photomultiplier tube. For imaging-based ECL detection, we used a charge-coupled device (CCD) camera (Falcon II, Raptor Photonics) equipped with a focusing zoom lens (FB0745, Guilin FT-OPTO). Screen-printed, single-use electrodes were used: Au electrodes (Cat. #220 AT, Metrohm), Pt electrodes (Cat. #550, Metrohm), and carbon electrodes (Cat. #C110, Metrohm). Refer to Table S4 for the summary of the experimental conditions for all ECL measurements.

Molecular simulation

We used the Gaussian 16 program to calculate the HOMO of cationic radicals. The calculation was based on DFT, using the B3LYP functional and the 6-311G(d,p) basis set. The pK_a values of the methyl group in DMAP were predicted by the Jaguar pK_a calculation module in Schröddinger (Schrödinger K.K.).

Mass spectroscopy

We performed high-resolution mass spectrometric experiments using the Orbitrap Exploris 480 mass spectrometer via direct

infusion of samples without further dilution. Mass spectrometric parameters were set as follows: 3.5 kV (electrospray voltage), 325°C (temperature of an ion transfer tube), and 30,000 (mass resolving power at m/z = 200).

EPR measurements

We conducted the spin-trapping EPR experiment by introducing DMPO as a spin trap into a solution containing 4-DMAP (10 mM) and formic acid at pH 6.8. The solution was then subjected to electrolysis at 1.2 V (vs. Ag/AgCl) for 1 h under an Ar-saturated atmosphere to minimize the oxygen content. EPR spectra were obtained using a Bruker Elexsys spectrometer equipped with an ER4103 TM cavity and operating at X-band.

EPR simulation

The initial geometry optimization of each candidate molecule was performed using DFT with the B3LYP functional and the def2-SVP basis set implemented in ORCA 4.2.1.[38–41] The optimized geometries obtained in vacuo were used for all calculations throughout this study, and no implicit or explicit solvent environment was considered. The EPR spin Hamiltonian parameters were computed through single-point DFT calculations using the B3LYP functional and the def2-TZVPD basis set, which is a balanced polarized triple-zeta basis set with diffuse and polarized functions.[39,42] Next, the simulations of continuous-wave EPR (CW EPR) spectra were conducted using the EasySpin package (version 5.2.35)[43] and MATLAB 9.13.0 toolbox. To account for the presence of overlapping hyperfine splittings, we incorporated an isotropic Gaussian line broadening. The input parameters for EasySpin simulations included the anisotropic g-factors, the anisotropic hyperfine couplings of the relevant ^{1}H and ^{14}N atoms from the DFT simulation, and a fitting parameter for the peak-to-peak linewidth to account for line broadening. The same fitting parameters were used for comparing the simulated EPR spectra of all candidate molecules with the experimental spectrum.

Material stability test

We prepared the test solutions by dissolving TPrA (10 mM) or 4-DMAP (10 mM) in a 0.2 M phosphate buffer. Subsequently, the prepared samples were stored at ambient conditions (20°C) and utilized for ECL measurements with $[Ru(bpy)_3]^{2+}$ (1 μM).

ECL flow cell assay

We designed and fabricated a flow cell consisting of a top cover and a microfluidic channel. The top cover was made of a 3-mm acrylic sheet, and the microfluidic channel was made of a polyethylene terephthalate (PET) film (127-μm thickness; McMaster-Carr) coated with a double-sided tape (467MP, 3M). We patterned the acrylic sheet and the PET film using a laser cutter (Fusion Edge 12, Epilog Laser) and assembled the flow cell by bonding cut parts on the top side of an electrode. We also attached a neodymium magnet (6-mm diameter) under the working electrode and connected the flow cell to a syringe pump. We introduced ECL reagents to the flow cell and measured ECL signals using an EM-CCD camera (Falcon II, Raptor Photonics).

EV production and characterization

We seeded SW480 cells (American Type Culture Collection) in a T175 flask and cultured them in vendor-recommended media supplemented with 1% exo-free fetal bovine serum (Thermofisher). For EV collection, cell-culture supernatants (100 mL) were collected and centrifuged at 300 × *g* for 10 min. After centrifugation, supernatants were collected and centrifuged again at 2,000 × *g* for 10 min. Finally, clear supernatants were filtered through a 0.22-μm membrane filter (cat#430767, Corning), and the filtrates were concentrated using centrifugal filters (10 kDa cutoff; Centricon-70, Millipore Sigma). We measured EV size and concentrations through nanoparticle tracking analysis (NTA). NanoSight LM10 (Malvern), which was equipped with a 405 nm laser, was employed for the analysis. Samples were diluted in fPBS to obtain the recommended particle concentration (25–100 particles/frame). For each test sample, we recorded three 30-s videos (camera level, 14) and analyzed the recorded videos using NTA software (version 3.2) at a detection threshold of 3.

Antibody conjugation with ECL labels

We added 10 μL of antibody (anti-human IgG (1 mg/mL), anti-CD63 (1 mg/mL), anti-EpCAM (1 mg/mL), and anti-EGFR (1 mg/mL)) into 187.5 μL of 1× PBS. Then, 2.5 μL of Ru(bpy)$_2$(mcbpy-*O*-Su-ester)(PF$_6$)$_2$ solution (5 mg/mL in ethanol, Abcam) was added to the antibody solution. We incubated the mixture solution using a Hulamixer for 1 h at 25°C in a dark condition. Afterward, we washed the mixture solution 2 times using a 3 KDa Amicon filter (Millipore Sigma). We diluted the collected solution to 10 μg/mL in 0.1% BSA and stored it at −20°C until use.

Preparation of immunomagnetic beads for EV detection

We used magnetic beads coated with streptavidin (Dynabeads M-280 Streptavidin, Invitrogen). Beads were magnetically washed three times in PBS and resuspended in PBS (1×10^9 bead/mL). We next mixed beads (100 μL) with biotinylated CD63 antibody (20 μg) and incubated the mixture on a rotating mixer (2 h, 20°C). The reacted beads were triple washed in PBS and resuspended in PBS containing SuperBlock (Thermo Fisher Scientific). The final bead concentration was about 10^9 beads/mL.

ECL assay to detect EVs in plasma samples

This study was approved by the Institutional Review Board of Massachusetts General Hospital (IRB number: 2019P003441, PI: Hakho Lee). Informed consent was obtained from all subjects. To capture EVs, we mixed samples (100 μL of EV-spiked PBS or 100 μL of plasma) with CD63-specific magnetic beads (2 μL, 10^9 beads/mL). After 30-min incubation (20°C), we magnetically washed the beads twice in PBS containing 0.05% Tween 20. For target marker labeling, we collected the beads (solid contents) and added a probe antibody (30 μL) conjugated with $[Ru(bpy)_3]^{2+}$. After 15-min incubation (20°C), we magnetically washed the beads three times in PBS and resuspended them in PBS (30 μL). ECL measurements were then carried out using the same protocol as in the nAb assay.

Preparation of immunomagnetic beads for antibody detection

We used magnetic beads with epoxy functional groups (Dynabeads M-270 epoxy, Invitrogen). Beads were washed three times in 0.1 M sodium phosphate solution, magnetically collected, and resuspended in 0.1 M sodium phosphate solution (1×10^9 bead/mL). The bead solution (100 μL) was then mixed antibody against S-protein (20 μg) in ammonium sulfate (3 M, 100 μL). The mixture was incubated (8 h, 4°C) on a rotating mixer. Finally, antibody-conjugated beads were collected and resuspended in PBS (50 μL). The final bead concentration was about 10^9 beads/mL.

ECL assay to detect nAbs in saliva

This study was approved by the Institutional Review Board of Massachusetts General Hospital (IRB number: 2019P003472, PI: Hakho Lee). Informed consent was obtained from all subjects. We used a saliva sampling kit (Salivatte, Sarstedt) to obtain saliva samples from volunteers. Volunteers chewed a polymeric swab (1 min) and placed it into the collection tube. The tube with the swab was centrifuged (3200 ×g, 2 min) to collect saliva. We mixed antibody-conjugated (against S protein) magnetic beads (2 μL, 10^9 bead/mL) with 80 μL of S protein (100 ng/mL, S protein spiked PBS) and 30 μL of human saliva. We then reacted the mixture for 30 min at 20°C on a rotating mixer. After the reaction, the beads were washed twice in PBS containing 0.05% Tween 20 and magnetically collected. Subsequently, we added human IgG antibodies (30 μL, 5 μg/mL) conjugated with $[Ru(bpy)_3]^{2+}$. The mixture was placed on a rotating mixer (30 min, 20°C). Finally, the beads were triple washed in PBS and resuspended (30 μL PBS). For ECL measurements, we mixed 7 μL of the bead solution with coreactant (43 μL), either 10 mM 4-DMAP or 10 mM TPrA, and dispensed the mixture on a working electrode. After 1 min incubation (20°C), we applied a repeated pulse (1.2 V, 0.1-s duration).

RESOURCE AVAILABILITY

Lead contact

Requests for further information and resources should be directed to and will be fulfilled by the lead contact, Ik-Soo Shin (extant@ssu.ac.kr).

Materials availability

This study did not generate new unique materials.

Data and code availability

- All data supporting the results in this study are available within the paper and its supplementary information. Additional data are available from the corresponding authors upon reasonable request.
- This paper does not report original code.
- Any additional information required to reanalyze the data reported in this paper, including the raw patient datasets generated and analyzed during the study are available from the corresponding authors on reasonable request, subject to approval from the Institutional Review Board of Massachusetts General Hospital.

ACKNOWLEDGMENTS

This work was supported in part by NIH R01CA264363 (H.L.), R01CA239078 (H.L.), R01CA237500 (H.L.), R21CA267222 (H.L.), U01CA284982 (H.L.), R01HL163513 (H.L.), U01CA279858 (H.L.), and Ministry of Science and ICT of Korea (RS-2024-00354654; I.-S.S.).

AUTHOR CONTRIBUTIONS

Y.K.C., S.-H.J., Hakho L., and I.-S.S. conceived the project. Y.K.C., S.-H.J., J.Y.P., H.K., B.-J.S., Haeun L., H.-K.W., and J.H.P. carried out the experiments. Y.K.C., S.-H.J., J.H.K., J.-S.K., Hakho L., and I.-S.S. analyzed the data. K.N. and S.S.K. performed EPR simulation. Y.K.C., S.-H.J., Hakho L., and I.-S.S. wrote the manuscript with input from all authors. All authors approved the final version of the article.

DECLARATION OF INTERESTS

I.-S.S. declares the filing of a patent (US20190346434A1) that was assigned to and handled by Soongsil University.

SUPPLEMENTAL INFORMATION

Supplemental information can be found online at https://doi.org/10.1016/j.xcrp.2025.102864.

Received: April 22, 2025
Revised: June 24, 2025
Accepted: September 3, 2025
Published: September 26, 2025

REFERENCES

1. Guo, W., Ding, H., Gu, C., Liu, Y., Jiang, X., Su, B., and Shao, Y. (2018). Potential-Resolved Multicolor Electrochemiluminescence for Multiplex Immunoassay in a Single Sample. J. Am. Chem. Soc. *140*, 15904–15915. https://doi.org/10.1021/jacs.8b09422.
2. Dong, J., Lu, Y., Xu, Y., Chen, F., Yang, J., Chen, Y., and Feng, J. (2021). Direct imaging of single-molecule electrochemical reactions in solution. Nature *596*, 244–249. https://doi.org/10.1038/s41586-021-03715-9.
3. Voci, S., Goudeau, B., Valenti, G., Lesch, A., Jović, M., Rapino, S., Paolucci, F., Arbault, S., and Sojic, N. (2018). Surface-Confined Electrochemiluminescence Microscopy of Cell Membranes. J. Am. Chem. Soc. *140*, 14753–14760. https://doi.org/10.1021/jacs.8b08080.
4. Ege, D., Becker, W.G., and Bard, A.J. (1984). Electrogenerated chemiluminescent determination of Ru(bpy)3(2+) at low levels. Anal. Chem. *56*, 2413–2417. https://doi.org/10.1021/ac00277a036.
5. Leland, J.K., and Powell, M.J. (1990). Electrogenerated Chemiluminescence: An Oxidative-Reduction Type ECL Reaction Sequence Using Tripropyl Amine. J. Electrochem. Soc. *137*, 3127–3131. https://doi.org/10.1149/1.2086171.
6. Welter, S., Brunner, K., Hofstraat, J.W., and De Cola, L. (2003). Electroluminescent device with reversible switching between red and green emission. Nature *421*, 54–57. https://doi.org/10.1038/nature01309.
7. Fosdick, S.E., Knust, K.N., Scida, K., and Crooks, R.M. (2013). Bipolar electrochemistry. Angew. Chem. Int. Ed. *52*, 10438–10456. https://doi.org/10.1002/anie.201300947.
8. Ino, K., Yaegaki, R., Hiramoto, K., Nashimoto, Y., and Shiku, H. (2020). Closed Bipolar Electrode Array for On-Chip Analysis of Cellular Respiration by Cell Aggregates. ACS Sens. *5*, 740–745. https://doi.org/10.1021/acssensors.9b02061.
9. Richter, M.M. (2004). Electrochemiluminescence (ECL). Chem. Rev. *104*, 3003–3036. https://doi.org/10.1021/cr020373d.
10. Lee, W.-Y. (1997). Tris (2,2?-bipyridyl)ruthenium(II) electrogenerated chemiluminescence in analytical science. Mikrochim. Acta *127*, 19–39. https://doi.org/10.1007/bf01243160.

11. Zanut, A., Fiorani, A., Canola, S., Saito, T., Ziebart, N., Rapino, S., Rebeccani, S., Barbon, A., Irie, T., Josel, H.P., et al. (2020). Insights into the mechanism of coreactant electrochemiluminescence facilitating enhanced bioanalytical performance. Nat. Commun. *11*, 2668. https://doi.org/10.1038/s41467-020-16476-2.

12. Shin, I.S., Kang, Y.T., Lee, J.K., Kim, H., Kim, T.H., and Kim, J.S. (2011). Evaluation of electrogenerated chemiluminescence from a neutral Ir(III) complex for quantitative analysis in flowing streams. Analyst *136*, 2151–2155. https://doi.org/10.1039/c1an15045f.

13. Jin, Y., Kang, Q., Guo, X., Zhang, B., Shen, D., and Zou, G. (2018). Electrochemical-Signal-Amplification Strategy for an Electrochemiluminescence Immunoassay with g-C_3N_4 as Tags. Anal. Chem. *90*, 12930–12936. https://doi.org/10.1021/acs.analchem.8b03554.

14. Ding, C., Zhang, W., Wang, W., Chen, Y., and Li, X. (2015). Amplification strategies using electrochemiluminescence biosensors for the detection of DNA, bioactive molecules and cancer biomarkers. TrAC, Trends Anal. Chem. *65*, 137–150. https://doi.org/10.1016/j.trac.2014.10.015.

15. Lippi, G., Henry, B.M., and Adeli, K. (2022). Diagnostic performance of the fully automated Roche Elecsys SARS-CoV-2 antigen electrochemiluminescence immunoassay: a pooled analysis. Clin. Chem. Lab. Med. *60*, 655–661. https://doi.org/10.1515/cclm-2022-0053.

16. Liu, X., Shi, L., Niu, W., Li, H., and Xu, G. (2007). Environmentally friendly and highly sensitive ruthenium(II) tris(2,2'-bipyridyl) electrochemiluminescent system using 2-(dibutylamino)ethanol as co-reactant. Angew. Chem. Int. Ed. Engl. *46*, 421–424. https://doi.org/10.1002/anie.200603491.

17. Zu, Y., and Bard, A.J. (2001). Electrogenerated chemiluminescence. 67. Dependence of light emission of the tris(2,2')bipyridylruthenium(II)/tripropylamine system on electrode surface hydrophobicity. Anal. Chem. *73*, 3960–3964. https://doi.org/10.1021/ac010230b.

18. Zanarini, S., Rampazzo, E., Ciana, L.D., Marcaccio, M., Marzocchi, E., Montalti, M., Paolucci, F., and Prodi, L. (2009). Ru(bpy)(3) covalently doped silica nanoparticles as multicenter tunable structures for electrochemiluminescence amplification. J. Am. Chem. Soc. *131*, 2260–2267. https://doi.org/10.1021/ja8077158.

19. Oyama, N., Komori, K., and Hatozaki, O. (2001). Electrochemiluminescence reactions of metal complexes immobilized on surface of a. In magnetic microbead Studies in Surface Science and Catalysis, 132, Y. Iwasawa, N. Oyama, and H. Kunieda, eds. (Elsevier), pp. 427–430.

20. Smith, P.J., and Mann, C.K. (1969). Electrochemical dealkylation of aliphatic amines. J. Org. Chem. *34*, 1821–1826. https://doi.org/10.1021/jo01258a063.

21. Carrara, S., Arcudi, F., Prato, M., and De Cola, L. (2017). Amine-Rich Nitrogen-Doped Carbon Nanodots as a Platform for Self-Enhancing Electrochemiluminescence. Angew. Chem. Int. Ed. Engl. *56*, 4757–4761. https://doi.org/10.1002/anie.201611879.

22. Ma, Y., Colin, C., Descamps, J., Arbault, S., and Sojic, N. (2021). Shadow Electrochemiluminescence Microscopy of Single Mitochondria. Angew. Chem. Int. Ed. Engl. *60*, 18742–18749. https://doi.org/10.1002/anie.202105867.

23. Wang, Y., Ding, J., Zhou, P., Liu, J., Qiao, Z., Yu, K., Jiang, J., and Su, B. (2023). Electrochemiluminescence Distance and Reactivity of Coreactants Determine the Sensitivity of Bead-Based Immunoassays. Angew. Chem. Int. Ed. Engl. *62*, e202216525. https://doi.org/10.1002/anie.202216525.

24. Galabov, B., Nalbantova, D., Schleyer, P.V.R., and Schaefer, H.F. (2016). Electrophilic Aromatic Substitution: New Insights into an Old Class of Reactions. Acc. Chem. Res. *49*, 1191–1199. https://doi.org/10.1021/acs.accounts.6b00120.

25. Li, S., Tang, J., Shi, Y., Yan, M., Fu, Y., Su, Z., Xu, J., Xue, W., Zheng, X., Ge, Y., et al. (2024). C3 Selective chalcogenation and fluorination of pyridine using classic Zincke imine intermediates. Nat. Commun. *15*, 7420. https://doi.org/10.1038/s41467-024-51452-0.

26. Valenti, G., Fiorani, A., Li, H., Sojic, N., and Paolucci, F. (2016). Essential Role of Electrode Materials in Electrochemiluminescence Applications. Chemelectrochem *3*, 1990–1997. https://doi.org/10.1002/celc.201600602.

27. Noffsinger, J.B., and Danielson, N.D. (1987). Generation of chemiluminescence upon reaction of aliphatic amines with tris(2,2'-bipyridine) ruthenium(III). Anal. Chem. *59*, 865–868. https://doi.org/10.1021/ac00133a017.

28. Daviddi, E., Oleinick, A., Svir, I., Valenti, G., Paolucci, F., and Amatore, C. (2017). Theory and Simulation for Optimising Electrogenerated Chemiluminescence from Tris(2,2′-bipyridine)-ruthenium(II)-Doped Silica Nanoparticles and Tripropylamine. Chemelectrochem *4*, 1719–1730. https://doi.org/10.1002/celc.201600892.

29. Valenti, G., Scarabino, S., Goudeau, B., Lesch, A., Jović, M., Villani, E., Sentic, M., Rapino, S., Arbault, S., Paolucci, F., and Sojic, N. (2017). Single Cell Electrochemiluminescence Imaging: From the Proof-of-Concept to Disposable Device-Based Analysis. J. Am. Chem. Soc. *139*, 16830–16837. https://doi.org/10.1021/jacs.7b09260.

30. Shao, H., Im, H., Castro, C.M., Breakefield, X., Weissleder, R., and Lee, H. (2018). New Technologies for Analysis of Extracellular Vesicles. Chem. Rev. *118*, 1917–1950. https://doi.org/10.1021/acs.chemrev.7b00534.

31. Park, J., Park, J.S., Huang, C.H., Jo, A., Cook, K., Wang, R., Lin, H.Y., Van Deun, J., Li, H., Min, J., et al. (2021). An integrated magneto-electrochemical device for the rapid profiling of tumour extracellular vesicles from blood plasma. Nat. Biomed. Eng. *5*, 678–689. https://doi.org/10.1038/s41551-021-00752-7.

32. Im, H., Shao, H., Park, Y.I., Peterson, V.M., Castro, C.M., Weissleder, R., and Lee, H. (2014). Label-free detection and molecular profiling of exosomes with a nano-plasmonic sensor. Nat. Biotechnol. *32*, 490–495. https://doi.org/10.1038/nbt.2886.

33. Lee, K., Fraser, K., Ghaddar, B., Yang, K., Kim, E., Balaj, L., Chiocca, E.A., Breakefield, X.O., Lee, H., and Weissleder, R. (2018). Multiplexed Profiling of Single Extracellular Vesicles. ACS Nano *12*, 494–503. https://doi.org/10.1021/acsnano.7b07060.

34. Najjar, D., Rainbow, J., Sharma Timilsina, S., Jolly, P., de Puig, H., Yafia, M., Durr, N., Sallum, H., Alter, G., Li, J.Z., et al. (2022). A lab-on-a-chip for the concurrent electrochemical detection of SARS-CoV-2 RNA and anti-SARS-CoV-2 antibodies in saliva and plasma. Nat. Biomed. Eng. *6*, 968–978. https://doi.org/10.1038/s41551-022-00919-w.

35. Ketas, T.J., Chaturbhuj, D., Portillo, V.M.C., Francomano, E., Golden, E., Chandrasekhar, S., Debnath, G., Díaz-Tapia, R., Yasmeen, A., Kramer, K.D., et al. (2021). Antibody Responses to SARS-CoV-2 mRNA Vaccines Are Detectable in Saliva. Pathog. Immun. *6*, 116–134. https://doi.org/10.20411/pai.v6i1.441.

36. Miao, W., Choi, J.P., and Bard, A.J. (2002). Electrogenerated chemiluminescence 69: the tris(2,2'-bipyridine)ruthenium(II), (Ru(bpy)3(2+))/tri-n-propylamine (TPrA) system revisited-a new route involving TPrA*+ cation radicals. J. Am. Chem. Soc. *124*, 14478–14485. https://doi.org/10.1021/ja027532v.

37. Kanoufi, F., Zu, Y., and Bard, A.J. (2001). Homogeneous Oxidation of Trialkylamines by Metal Complexes and Its Impact on Electrogenerated Chemiluminescence in the Trialkylamine/$Ru(bpy)_3^{2+}$ System. J. Phys. Chem. B *105*, 210–216. https://doi.org/10.1021/jp002880.

38. Stephens, P.J., Devlin, F.J., Chabalowski, C.F., and Frisch, M.J. (1994). Ab Initio Calculation of Vibrational Absorption and Circular Dichroism Spectra Using Density Functional Force Fields. J. Phys. Chem. *98*, 11623–11627. https://doi.org/10.1021/j100096a001.

39. Weigend, F., and Ahlrichs, R. (2005). Balanced basis sets of split valence, triple zeta valence and quadruple zeta valence quality for H to Rn: Design and assessment of accuracy. Phys. Chem. Chem. Phys. *7*, 3297–3305. https://doi.org/10.1039/b508541a.

40. Schäfer, A., Horn, H., and Ahlrichs, R. (1992). Fully optimized contracted Gaussian basis sets for atoms Li to Kr. J. Chem. Phys. *97*, 2571–2577. https://doi.org/10.1063/1.463096.

41. Neese, F. (2012). The ORCA program system. WIREs Comput. Mol. Sci. *2*, 73–78. https://doi.org/10.1002/wcms.81.

42. Rappoport, D., and Furche, F. (2010). Property-optimized gaussian basis sets for molecular response calculations. J. Chem. Phys. *133*, 134105. https://doi.org/10.1063/1.3484283.

43. Stoll, S., and Schweiger, A. (2006). EasySpin, a comprehensive software package for spectral simulation and analysis in EPR. J. Magn. Reson. *178*, 42–55. https://doi.org/10.1016/j.jmr.2005.08.013.